

Proximity effects in bilayer graphene on monolayer WSe₂: Field-effect spin-valley locking, spin-orbit valve, and spin transistor

Martin Gmitra and Jaroslav Fabian

*Institute for Theoretical Physics, University of Regensburg,
93040 Regensburg, Germany*

Proximity orbital and spin-orbit effects of bilayer graphene on monolayer WSe₂ are investigated from first-principles. We find that the built-in electric field induces an orbital band gap of about 10 meV in bilayer graphene. Remarkably, the proximity spin-orbit splitting for holes is two orders of magnitude—the spin-orbit splitting of the valence band at K is about 2 meV—more than for electrons. Effectively, holes experience spin-valley locking due to the strong proximity of the lower graphene layer to WSe₂. However, applying an external transverse electric field of some 1 V/nm, countering the built-in field of the heterostructure, completely reverses this effect and allows, instead for holes, electrons to be spin-valley locked with 2 meV spin-orbit splitting. Such a behavior constitutes a highly efficient field-effect spin-orbit valve, making bilayer graphene on WSe₂ a potential platform for a field-effect spin transistor.

PACS numbers: 72.80.Vp, 71.70.Ej, 73.22.Pr

Keywords: spintronics, graphene, transition-metal dichalcogenides, heterostructures, spin-orbit coupling

Introduction. Heterostructures of two-dimensional materials can fundamentally alter their properties due to proximity effects. For example, graphene on transition metal dichalcogenides (TMDC) can serve as a new platform for optospintronics [1], as recently also demonstrated experimentally [2, 3] promoting graphene spintronics [4] towards applications [5, 6]. Bilayer graphene (BLG) on TMDC is expected to represent even more technologically feasible approach as it allows a precise (sub meV) control of the chemical potential—due to much smaller Fermi level fluctuations [7]—than in single layer graphene [8].

There have recently been intensive efforts to predict realistic graphene structures, through enhancing spin-orbit coupling by decorating graphene with adatoms, that would exhibit quantum spin (and anomalous) Hall effects [9–12], introduced by Kane and Mele [13] as a precursor of topological insulators [14–16]. Unlike promising approaches to enhance spin-orbit coupling via adatoms [17, 18], demonstrated already experimentally by the giant spin Hall effect signals [19, 20], van der Waals heterostructures provide more robust control towards technological reproducibility of devices. Recently, proximity effects in graphene on the whole family of TMDCs as potential substrates for graphene were explored theoretically [21, 22]. An enhancement of proximity spin-orbit coupling, of about 1 meV, was predicted, which is giant compared to bare graphene, in which spin-orbit coupling is about 10 μ eV [23]. The special case is graphene on WSe₂, where the predicted band inversion was proposed to lead to novel topological properties, [22, 24, 25], and giant spin relaxation anisotropy [26]. Important, graphene/TMDCs has already been grown [27–30] and investigated for transport [20, 24, 31–33], optoelectronics [34] as well as considered for technological

applications [35–38].

A BLG can exhibit an electronic bandgap in the presence of a transverse electric field [39–42]. The tunable bandgap enables a variety of different device concepts with novel functionalities for electronic, optoelectronic, and sensor applications. There were several proposals to increase the ON/OFF ratio in gated BLG, introducing a tunnel field-effect transistor [43] or a field effect transistor by adsorbate doping [44] to establish a displacement field. Also, BLG/TMDC heterostructures can potentially realize predicted topological insulating phases protected by no-valley mixing symmetry, featuring quantum valley Hall effects and chiral edge states [45–47].

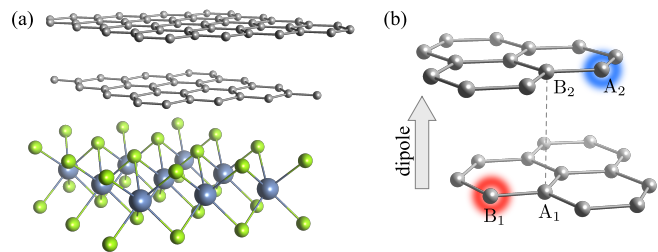


FIG. 1. (a) Atomic structure of bilayer graphene on a monolayer WSe₂ (supercell). (b) Sketch of bilayer graphene with atom labels forming a bare unit cell in Bernal stacking. Orbitals on non-dimer atoms B₁ and A₂ form the low energy valence and conduction bands in the electronic structure of bilayer graphene, with B₁ being closer to WSe₂.

In this paper we find, by performing first-principles investigations, that in a BLG/WSe₂ heterostructure a displacement field emerges intrinsically, allowing for a highly efficient electric control of proximity effects. Specifically, we find that (i) The intrinsic bandgap, which is about 10 meV, can be enhanced, reduced to zero, or reversed

by typical experimental electric fields on the order of 1 V/nm; (ii) The spin-orbit coupling of the valence band is giant, about 2 meV, being two orders of magnitude greater than in the conduction band, which is similar to intrinsic BLG [48]. The reason for this huge disparity is that the valence band is formed by non-dimer carbon atom orbitals in the bottom layer adjacent to WSe₂, while the conduction band is formed by non-dimer orbitals in the top layer, where proximity effects are naturally weak (the pair of atoms vertically connected we call dimer, the other pair non-dimer); (iii) The spin-orbit coupling of the valence bands is of spin-valley locking character, inherited from the monolayer WSe₂ substrate; (iv) A transverse electric field can turn spin-orbit coupling and spin-valley locking of electrons effectively on (and holes off), by countering the built-in field. We call this effect *spin-orbit valve*. Connecting the spin-orbit to spin relaxation, the two decades of spin-orbit coupling translates into four orders of magnitude change in spin relaxation. Such a strong field-effect spin relaxation effect would be an ideal platform for the spin transistor of Hall and Flatte [49].

Electronic band structure of bilayer graphene on WSe₂.

The electronic structure calculations and structural relaxation were performed by Quantum ESPRESSO[50]; see Supplemental material [51] for further details [52–56]. In Fig. 2(a) we show the calculated electronic band structure of BLG on monolayer WSe₂ along high symmetry lines. The parabolic band dispersion of high and low energy bands close to the Fermi level resembles bare BLG [42, 57]. The high energy bands originate from the orbitals in dimer A₁ and B₂ atoms connected by direct interlayer hopping [42, 57] which shifts the bands some 400 meV off the Fermi level, far enough to ignore these bands for transport.

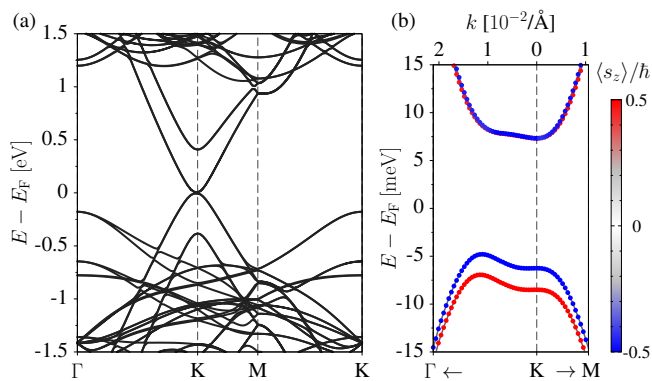


FIG. 2. (Color online) (a) Calculated electronic band structure of bilayer graphene on monolayer WSe₂. (b) Zoom to the fine structure of the low energy bands close to the Fermi level. Bands with positive (negative) z component of the spin are shown in red (blue).

The proximity effects influence mainly the low energy

bands of BLG. These bands originate from the p_z orbitals on non-dimer B₁ and A₂ atoms which form the valence and conduction band edges, respectively. An indirect bandgap of 12 meV, see Fig. 2(b), is opened due to proximity induced intrinsic electric field built across the BLG/WSe₂ heterostructure. The transverse field points from WSe₂ towards the BLG (we call this direction positive) with the amplitude of 0.267 V/nm. This is why B₁ electrons have lower energy, and form the valence band, while A₂ electrons have higher energy and form the conduction band. Apart from the orbital effect, the proximity also induces significant spin splitting of 2.2 meV in the valence band, seen in Fig. 2(b). This makes sense as B₁ atoms, responsible for the valence band, are close to WSe₂ and experience the proximity effects most.

Proximity effects in the conduction band are essentially non-existent, since A₂ atoms sit far from WSe₂. The numerical value of the spin-orbit splitting for the conduction band obtained by Quantum ESPRESSO is too small (about 3 μ eV), as d orbitals are not properly treated by the method. We know that in pristine BLG spin-orbit splitting should be about 24 μ eV, due to the presence of d orbitals [48]. We can safely assume that this value, (perhaps up to 10% higher or lower due to the proximity effects on p orbitals), of spin-orbit splitting is there for BLG on WSe₂. We conclude that holes experience spin-orbit coupling (2 meV) two orders of magnitude higher than electrons (20 μ eV). A recent experiment has observed Shubnikov-de Haas oscillations in BLG on WSe₂ and found, by fitting the results to a simple band structure model, that spin-orbit proximity effect is about 10 meV [58]. Our results presented here disagree with this interpretation.

Valley spin-orbital effects. Inspecting energy dispersions near the K valley for the spin split low energy bands, we find pronounced trigonal warping, see color map plots in the k_x and k_y momentum plane in Fig. 3(a,c). Only the bottom spin-orbit split conduction band and the top valence bands are shown. The area of the plots corresponds to 0.5% of the full first Brillouin zone. The calculated spin expectation values for the low energy states are principally locked out-of-plane, see color map plots in Fig. 3(b,d).

For low carrier concentrations, the Fermi contours form three pockets along K- Γ directions. Further increase of doping level merges the three Fermi pockets with an emerging pocket centered at the K point. For the top valence band the merging occurs at the carrier concentration of $0.064 \times 10^{12} \text{ cm}^{-2}$. This is accompanied by the presence of a van Hove singularity in the density of states [51]. The same holds for the spin-orbit split band. The second van Hove singularity appears at the energy lower by 2.2 meV, that corresponds to the proximity induced spin-orbit splitting. A further increase of the Fermi level leads to a linear increase of the Fermi surface area and carrier concentrations [51]. Multiplying the

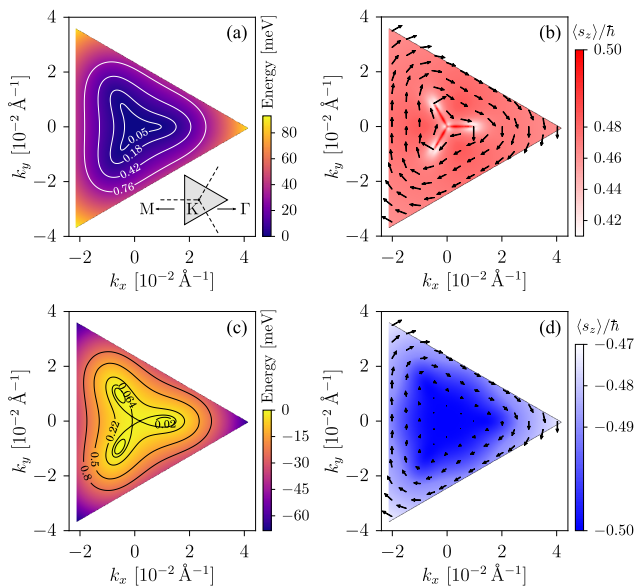


FIG. 3. (Color online) Calculated low energy electronic and spin properties of bilayer graphene on a monolayer WSe_2 . Shown are color map plots centered at K point representing 0.5% of the first Brillouin zone area for (a) energy of bottom conduction band measured from the conduction band edge. The contours correspond to carrier concentrations for 0.05, 0.18, 0.42 and $0.76 \times 10^{12} \text{ cm}^{-2}$. The inset depicts cut of the first Brillouin zone, shown by dashed lines, near the K point with directions towards M and Γ points. (b) Color map of z component spin expectation value with in-plane spin textures shown by the arrows. (c) Energy of the valence band measured from the valence band edge with contours showing carrier concentration of 0.02, 0.064, 0.22, 0.5 and $0.8 \times 10^{12} \text{ cm}^{-2}$, and (d) similar as in (b) but for the valence band.

calculated carrier concentration [51] by $\hbar/2e$ we can estimate the inverse frequency of the Shubnikov-de Haas oscillations, which for carrier concentrations of about $0.2 \times 10^{12} \text{ cm}^{-2}$ corresponds to 10 T^{-1} . The above mentioned experiment [58] observes similar values, although we cannot make a quantitative comparison due to the absence of carrier density data.

Spin-orbit valve. All electrical control of spin and orbital properties is a key feature for spintronics devices. Proximity induced spin-orbit coupling and the intrinsic electric polarization in BLG/ WSe_2 heterostructure can be efficiently controlled by an applied transverse electric field, as shows the plot of low energy band structures of BLG in the presence of applied electric fields in Fig. 4. Spontaneous polarization of the heterostructure induces a dipole in the simulated cell of about 0.7 Debye. This gives rise to a built-in transverse electric field of 0.267 V/nm which opens the electronic bandgap in BLG to the value of 12 meV . Applying a positive electric field the electronic gap further opens as the external field adds to the built-in internal field, see Fig. 4(e). However, when the applied field direction is reversed, the band gap

shrinks, and for the field of -0.25 V/nm which nearly compensates the intrinsic field, the gap fully closes, see Fig. 4(c). A further decrease (increase of the negative amplitude) of the field the bandgap opens again, but the characters of the valence and conduction bands flip and we get a spin-orbit valve!

The reason for this effect is simple. At zero applied electric field the spin-orbit splitting of the low energy valence bands originates from the bottom layer of BLG, adjacent to WSe_2 . More specifically, as already mentioned, the bands originate from the orbitals on carbon atoms B_1 . On the contrary, the low energy conduction bands are localized on the top (remote) BLG layer, specifically on atoms A_2 , see Fig. 4(d). The spin-orbit splitting of the valence bands is about 100 times larger near the K valley in comparison to the conduction band splitting. In the built-in electric field the bottom BLG layer experiences a lower potential than the top layer. Therefore, the valence (occupied) states originate from the bottom BLG layer, and the conduction (unoccupied) states from the top layer. For negative applied field of -0.5 V/nm the potential across the BLG reverses and band character switches, compare Fig. 4(a) and (d). Applying the external electric field induces also changes in the energy offset of the low energy bands with respect to the valence band maximum of the WSe_2 . For negative fields the BLG valence top is pushed down in energy and for the fields below -1 V/nm the valence top of the WSe_2 is above the valence top of BLG. In effect, BLG gets electron doped [51].

Bilayer graphene spin transistor. The proposed electrical switching of the spin-orbit splitting (either by changing the doping between electrons and holes, or by changing the electric field at a fixed chemical potential) presents a unique opportunity for a novel spin transistor design. We build on the spin transistor proposed by Hall and Flatté [49], which is an alternative to charge-based transistors by overcoming the $k_B T$ barrier for ON/OFF operations.

Suppose we have a half-metallic spin injector and detector, in an antiparallel configuration, connected to BLG proximitized to TMDC, see Fig. 5. We can control the spin-orbit coupling of the carriers in BLG by the spin-orbit valve effect. In the ON state, the spin-orbit coupling is high, spin relaxation is fast, and spin in the channel is reduced. Large current flows. In the OFF state, spin-orbit coupling is weak, spin relaxation slow, and spin in the channel is preserved. No current (in ideal case) flows.

The reason why this works is that spin relaxation depends on the square of spin-orbit coupling. BLG on WSe_2 should have spin relaxation due to the D'yakonov-Perel' [59], which is as a motional narrowing of the spin precession in a fluctuating (due to momentum scattering) emerging spin-orbit field $\mathbf{\Omega}(k)$. The spin-orbit splitting energy is proportional to $\hbar\Omega$, where Ω is the averaged

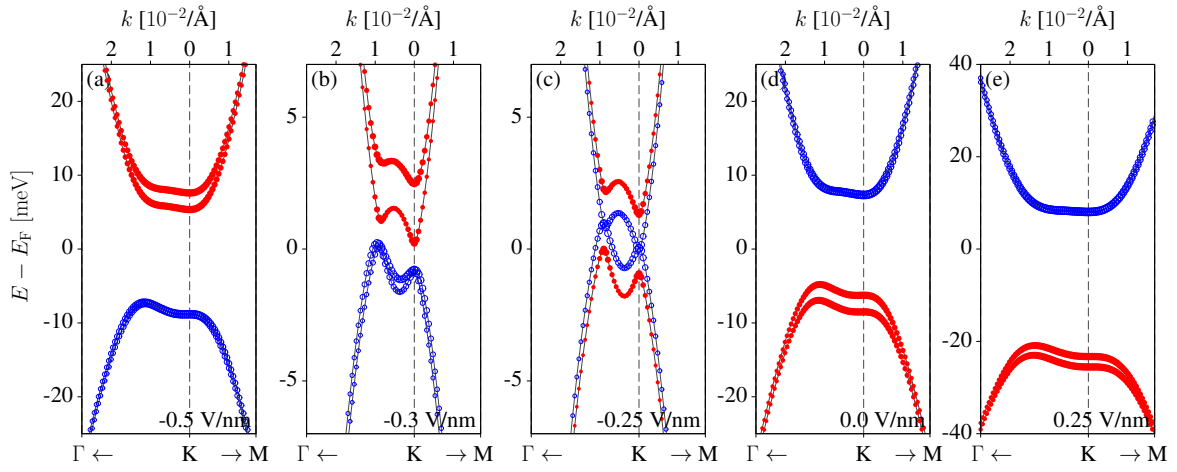


FIG. 4. (Color online) Calculated sublattice resolved band structures around K valley for transverse electric field of (a) -0.5 V/nm, (b) -0.2979 V/nm, (c) -0.25 V/nm, (d) zero field, and (e) 0.25 V/nm. The circles radii correspond to the probability of the state being localized on carbon atoms B_1 (red) filled circles and atoms A_2 (blue) open circles.

spin-orbit field for a Fermi contour. The spin relaxation rate is then given by $1/\tau_s = \Omega^2\tau$, where τ is the momentum relaxation time. Having calculated spin splitting at zero field of 2.2 meV for the low energy bands, we estimate the spin relaxation time of 1 ps, assuming typical value for $\tau = 100$ fs. Applying electric field of -0.5 V/nm, the band character switches and spin relaxation is reduced, which is comparable to what is seen in ultraclean graphene [60, 61] and BLG [62] encapsulated in hBN. The expected field-effect variation of spin relaxation time in BLG on WSe₂ is 4 orders of magnitude! Such a modulation is, to the best of our knowledge, unprecedented.

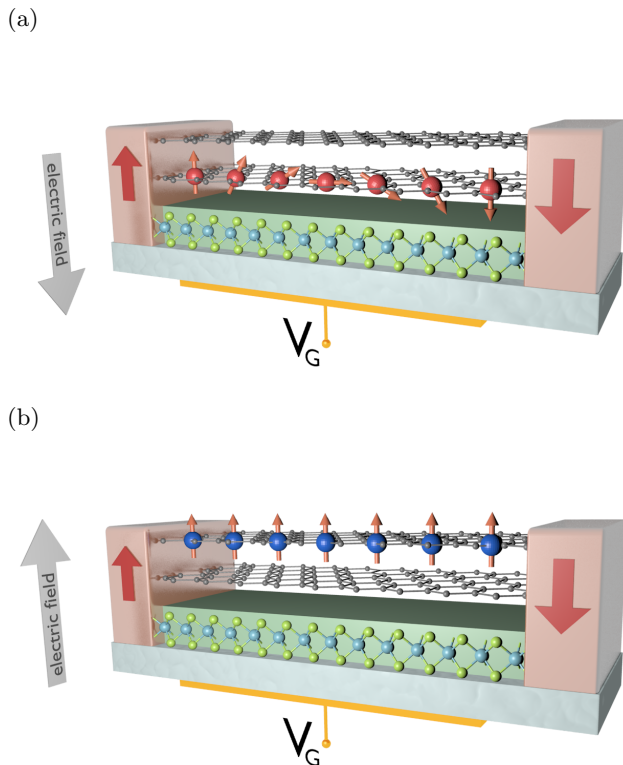


FIG. 5. (Color online) Schematics of spin-field effect transistor of bilayer graphene on a transition metal-dichalcogenide with two ferromagnets in antiparallel configuration acting as injector and detector of spins in the (a) spin-ON and (b) spin-OFF state.

In conclusion, we have studied from first principles the electronic structure of bilayer graphene on WSe₂. The most important finding is the field-effect spin-orbit valve, allowing for an efficient switching, by two orders of magnitude, of spin-orbit coupling of electrons and holes.

This work was supported by DFG SFB 689 and by the European Unions Horizon 2020 research and innovation programme under Grant agreement No. 696656. The authors gratefully acknowledge the Gauss Center for Supercomputing e.V. for providing computational resources on the GCS Supercomputer SuperMUC at Leib-

niz Supercomputing Center.

- [1] M. Gmitra and J. Fabian, *Phys. Rev. B* **92**, 155403 (2015).
- [2] A. Avsar, D. Unuchek, J. Liu, O. L. Sanchez, K. Watanabe, T. Taniguchi, B. Ozyilmaz, and A. Kis, arXiv:1705.10267 (2017).
- [3] Y. K. Luo, J. Xu, T. Zhu, G. Wu, E. J. McCormick, W. Zhan, M. R. Neupane, and R. K. Kawakami, *Nano Lett.* **17**, 3877 (2017).
- [4] W. Han, R. K. Kawakami, M. Gmitra, and J. Fabian, *Nat. Nanotechnol.* **9**, 794 (2014).
- [5] I. Žutić, J. Fabian, and S. Das Sarma, *Rev. Mod. Phys.* **76**, 323 (2004).
- [6] J. Fabian, A. Matos-Abiague, C. Ertler, P. Stano, and I. Žutić, *Acta Phys. Slovaca* **57**, 565 (2007).
- [7] G. M. Rutter, S. Jung, N. N. Klimov, D. B. Newell, N. B. Zhitenev, and J. A. Stroscio, *Nat Phys* **7**, 649 (2011).
- [8] J. Martin, N. Akerman, G. Ulbricht, T. Lohmann, J. H. Smet, K. von Klitzing, and A. Yacoby, *Nat Phys* **4**, 144 (2008).
- [9] Z. Qiao, S. A. Yang, W. Feng, W.-K. Tse, J. Ding, Y. Yao, J. Wang, and Q. Niu, *Phys. Rev. B* **82**, 161414 (2010).
- [10] C. Weeks, J. Hu, J. Alicea, M. Franz, and R. Wu, *Phys. Rev. X* **1**, 021001 (2011).
- [11] H. Zhang, C. Lazo, S. Blügel, S. Heinze, and Y. Mokrousov, *Phys. Rev. Lett.* **108**, 056802 (2012).
- [12] Z. Qiao, W. Ren, H. Chen, L. Bellaïche, Z. Zhang, A. MacDonald, and Q. Niu, *Phys. Rev. Lett.* **112**, 116404 (2014).
- [13] C. L. Kane and E. J. Mele, *Phys. Rev. Lett.* **95**, 146802 (2005).
- [14] B. A. Bernevig, T. L. Hughes, and S.-C. Zhang, *Science* **314**, 1757 (2006).
- [15] M. König, S. Wiedmann, C. Brüne, A. Roth, H. Buhmann, L. W. Molenkamp, X.-L. Qi, and S.-C. Zhang, *Science* **318**, 766 (2007).
- [16] H. Zhang, C.-X. Liu, X.-L. Qi, X. Dai, Z. Fang, and S.-C. Zhang, *Nat. Phys.* **5**, 438 (2009).
- [17] A. H. Castro Neto and F. Guinea, *Phys. Rev. Lett.* **103**, 026804 (2009).
- [18] M. Gmitra, D. Kochan, and J. Fabian, *Phys. Rev. Lett.* **110**, 246602 (2013).
- [19] J. Balakrishnan, G. Kok, W. Koon, M. Jaiswal, and A. H. C. Neto, *Nat. Phys.* **9**, 1 (2013).
- [20] A. Avsar, J. Y. Tan, T. Taychatanapat, J. Balakrishnan, G. K. W. Koon, Y. Yeo, J. Lahiri, A. Carvalho, A. S. Rodin, E. C. T. OFarrell, G. Eda, A. H. Castro Neto, and B. Özyilmaz, *Nat. Commun.* **5**, 4875 (2014).
- [21] T. P. Kaloni, L. Kou, T. Frauenheim, and U. Schwingschlögl, *Appl. Phys. Lett.* **105**, 233112 (2014).
- [22] M. Gmitra, D. Kochan, P. Högl, and J. Fabian, *Phys. Rev. B* **93**, 155104 (2016).
- [23] M. Gmitra, S. Konschuh, C. Ertler, C. Ambrosch-Draxl, and J. Fabian, *Phys. Rev. B* **80**, 235431 (2009).
- [24] Z. Wang, D.-K. Ki, H. Chen, H. Berger, A. H. MacDonald, and A. F. Morpurgo, *Nat. Commun.* **6**, 8339 (2015).
- [25] B. Yang, M.-F. Tu, J. Kim, Y. Wu, H. Wang, J. Alicea, R. Wu, M. Bockrath, and J. Shi, *2D Mater.* **3**, 031012 (2016).

- (2016).
- [26] A. W. Cummings, J. H. García, J. Fabian, and S. Roche, arXiv:1705.10972 (2017).
- [27] Y.-C. Lin, N. Lu, N. Perea-Lopez, J. Li, Z. Lin, X. Peng, C. H. Lee, C. Sun, L. Calderin, P. N. Browning, M. S. Bresnehan, M. J. Kim, T. S. Mayer, M. Terrones, and J. A. Robinson, *ACS Nano* **8**, 3715 (2014).
- [28] M.-Y. Lin, C.-E. Chang, C.-H. Wang, C.-F. Su, C. Chen, S.-C. Lee, and S.-Y. Lin, *Appl. Phys. Lett.* **105**, 073501 (2014).
- [29] M. M. Ugeda, A. J. Bradley, S.-F. Shi, F. H. da Jornada, Y. Zhang, D. Y. Qiu, W. Ruan, S.-K. Mo, Z. Hussain, Z.-X. Shen, F. Wang, S. G. Louie, and M. F. Crommie, *Nat. Mater.* **13**, 1091 (2014).
- [30] A. Azizi, S. Eichfeld, G. Geschwind, K. Zhang, B. Jiang, D. Mukherjee, L. Hossain, A. F. Piasecki, B. Kabius, J. A. Robinson, and N. Alem, *ACS Nano* **9**, 4882 (2015).
- [31] C.-P. Lu, G. Li, K. Watanabe, T. Taniguchi, and E. Y. Andrei, *Phys. Rev. Lett.* **113**, 156804 (2014).
- [32] S. Larentis, J. R. Tolsma, B. Fallahazad, D. C. Dillen, K. Kim, A. H. MacDonald, and E. Tutuc, *Nano Lett.* **14**, 2039 (2014).
- [33] S. Omar and B. J. van Wees, *Phys. Rev. B* **95**, 081404 (2017).
- [34] M. Massicotte, P. Schmidt, F. Violla, K. G. Schdler, A. Reserbat-Plantey, K. Watanabe, T. Taniguchi, K. J. Tielrooij, and F. H. L. Koppens, *Nat Nano* **11**, 42 (2016).
- [35] S. Bertolazzi, D. Krasnozhon, and A. Kis, *ACS Nano* **7**, 3246 (2013).
- [36] K. Roy, M. Padmanabhan, S. Goswami, T. P. Sai, G. Ramalingam, S. Raghavan, and A. Ghosh, *Nat. Nanotechnol.* **8**, 826 (2013).
- [37] W. Zhang, C.-P. Chuu, J.-K. Huang, C.-H. Chen, M.-L. Tsai, Y.-H. Chang, C.-T. Liang, Y.-Z. Chen, Y.-L. Chueh, J.-H. He, M.-Y. Chou, and L.-J. Li, *Sci. Rep.* **4**, 3826 (2014).
- [38] N. A. Kumar, M. A. Dar, R. Gul, and J. Baek, *Mater. Today* **18**, 286 (2015).
- [39] T. Ohta, A. Bostwick, T. Seyller, K. Horn, and E. Rotenberg, *Science* **313**, 951 (2006).
- [40] J. B. Oostinga, H. B. Heersche, X. Liu, A. F. Morpurgo, and L. M. K. Vandersypen, *Nat. Mater.* **7**, 151 (2008).
- [41] Y. Zhang, T.-T. Tang, C. Girit, Z. Hao, M. C. Martin, A. Zettl, M. F. Crommie, Y. R. Shen, and F. Wang, *Nature* **459**, 820 (2009).
- [42] E. McCann and V. I. Fal'ko, *Phys. Rev. Lett.* **96**, 086805 (2006).
- [43] G. Alymov, V. Vyurkov, V. Ryzhii, and D. Svintsov, *Scientific Reports* **6**, 24654 (2016).
- [44] B. N. Szafranek, D. Schall, M. Otto, D. Neumaier, and H. Kurz, *Nano Letters* **11**, 2640 (2011).
- [45] W. Yao, S. A. Yang, and Q. Niu, *Phys. Rev. Lett.* **102**, 096801 (2009).
- [46] F. Zhang, J. Jung, G. A. Fiete, Q. Niu, and A. H. MacDonald, *Phys. Rev. Lett.* **106**, 156801 (2011).
- [47] L. Ju, Z. Shi, N. Nair, Y. Lv, C. Jin, J. Velasco Jr, C. Ojeda-Aristizabal, H. A. Bechtel, M. C. Martin, A. Zettl, *J. Analytis*, and F. Wang, *Nature* **520**, 650 (2015).
- [48] S. Kunschuh, M. Gmitra, D. Kochan, and J. Fabian, *Phys. Rev. B* **85**, 115423 (2012).
- [49] K. C. Hall and M. E. Flatt, *Appl. Phys. Lett.* **88**, 162503 (2006).
- [50] P. Giannozzi and et al., *J.Phys.: Condens. Matter* **21**, 395502 (2009).
- [51] See Supplemental Material at <http://> for details of calculated density of states, carrier concentration, electrostatic quantities and spin-splitting of the low energy bilayer bands.
- [52] J. Hohenberg and W. Kohn, *Phys. Rev.* **136**, B864 (1964).
- [53] J. P. Perdew, K. Burke, and M. Ernzerhof, *Phys. Rev. Lett.* **77**, 3865 (1996).
- [54] S. Grimme, *J. Comput. Chem.* **27**, 1787 (2006).
- [55] V. Barone, M. Casarin, D. Forrer, M. Pavone, M. Sambri, and Vittadini, *J. Comput. Chem.* **30**, 934 (2009).
- [56] L. Bengtsson, *Phys. Rev. B* **59**, 12301 (1999).
- [57] J. Nilsson, A. H. Castro Neto, F. Guinea, and N. M. R. Peres, *Phys. Rev. B* **78**, 045405 (2008).
- [58] Z. Wang, D.-K. Ki, J. Y. Khoo, D. Mauro, H. Berger, L. S. Levitov, and A. F. Morpurgo, *Phys. Rev. X* **6**, 041020 (2016).
- [59] M. I. D'yakonov and V. I. Perel', *Fiz. Tverd. Tela* **13**, 3581 (1971), [*Sov. Phys. Solid State* **13**, 3023 (1972)].
- [60] M. H. D. Guimarães, P. J. Zomer, J. Ingla-Aynés, J. C. Brant, N. Tombros, and B. J. van Wees, *Phys. Rev. Lett.* **113**, 086602 (2014).
- [61] M. Gurrum, S. Omar, S. Zihlmann, P. Makk, C. Schönenberger, and B. J. van Wees, *Phys. Rev. B* **93**, 115441 (2016).
- [62] J. Ingla-Aynés, M. H. D. Guimarães, R. J. Meijerink, P. J. Zomer, and B. J. van Wees, *Phys. Rev. B* **92**, 201410 (2015).

SUPPLEMENTAL MATERIAL

The supplemental material provides further details of the calculational methods, calculated electronic properties, and electrostatic quantities. The information can be useful for further realization of proposed spin transistor concept in transport experiments.

Electronic structure of bilayer graphene (BLG) on WSe_2 was calculated by means of density functional theory [52]. We consider a supercell structural model, shown in Fig. 1(a) in the paper, containing a 3×3 cell of WSe_2 and a 4×4 cell of BLG in Bernal stacking, see Fig. 1(b) in the paper, with common lattice constant of 9.8934 Å. The supercell has 91 atoms. In such a quasi commensurate structure the residual strain results in a stretching of BLG by only 0.5%. Similar quasicommensurate superstructures of transition metal dichalcogenides have been grown on HOPG [29]. Electronic structure calculations and structural relaxation were performed within plane wave package Quantum ESPRESSO [50], using norm conserving pseudopotentials with kinetic energy cutoff of 60 Ry for wavefunctions. For the exchange-correlation potential we used the generalized gradient approximation [53]. The vacuum of 15 Å normal to the layer planes was considered. The first Brillouin zone was sampled with 545 k points. We estimated error in underestimation of the electronic bandgap from the convergence of the number of the used k points to 0.5 meV. We note that spin-orbit coupling properties for the used number of k points are well converged. The atomic positions were relaxed using the quasi-Newton algorithm based on the trust radius procedure including the van der Waals interaction which was treated within a semiempirical approach [54, 55]. The average interlayer distance 3.376 Å between BLG and WSe_2 is of van der Waals order. In our calculations we applied the dipole correction [56], which turned out to be crucial to get numerically accurate band offsets and internal electric fields.

In Fig. 6(a) we show calculated density of states for BLG on WSe_2 . Valence and conduction band edges are separated by the electronic gap of 12 meV. Near the edges pronounced van Hove singularities are present. They appear in pairs from each subband separately. As the valence bands are strongly spin split by 2.2 meV the peaks in the density of states are much more pronounced. The splitting of the conduction bands near the band edge is reduced 800 times. We note that the van Hove singularities appear at the energies at which the trigonal symmetric Fermi pockets extending along $\text{K}-\Gamma$ path near the band edges merge with the pocket centered at the K point.

Corresponding band resolved areas of the Fermi contours are shown in Fig. 6(b). For energies about 5 meV from the band edges the Fermi contour areas grow linearly. The nonlinearity near the band edge is related

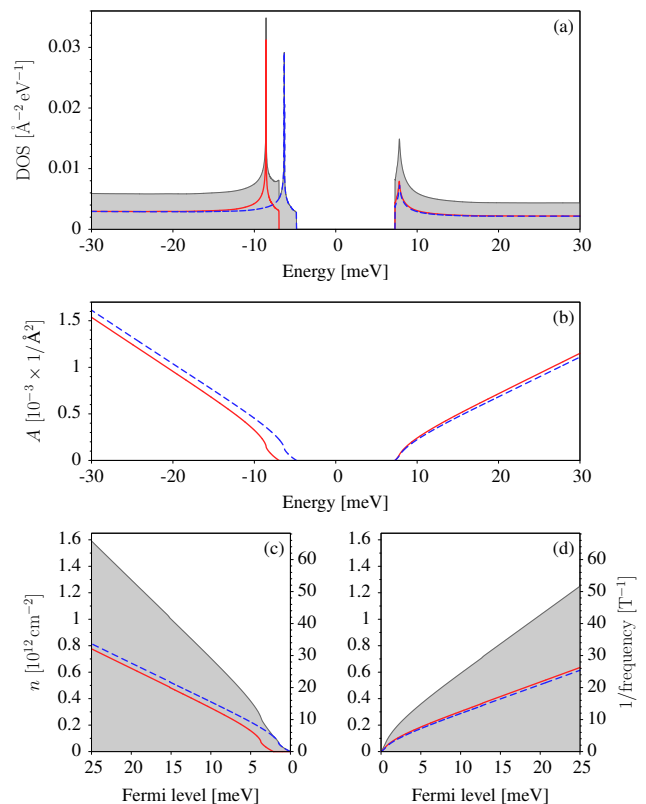


FIG. 6. Calculated (a) total density of states per unit of energy, shown by the shaded area. Contributions from spin split bands are shown by the lines. (b) Area of the Fermi contour band resolved as in (a). (c) Carrier concentration as a function of Fermi level for hole doping, shown by the shaded region with the corresponding band contribution shown by lines. (d) Carrier concentrations as in (c) but for electron doping.

with the existence of more than one Fermi pocket within a subband. Calculated band resolved carrier concentration shown in Fig. 6(c) and (d), show similar dependence on energy as the Fermi contours.

Across the BLG/ WSe_2 heterostructure induces in simulated cell of 2.12 nm^3 the dipole of 0.7 Debye with built-in electric field of 0.267 V/nm. Dependence of dipole as a function of the applied electric field (we note it is external field not the displacement field) is linear, see Fig. 7(a). The dipole is compensated by the negative field of about -0.3 V/nm. Applied electric field influences also energy offset of the BLG low energy states within the WSe_2 bandgap. In Fig. 7(b) we show energy offset of the BLG valence band at the K point and the valence band maximum of the WSe_2 . For field below -1 V/nm the valence band maximum of the WSe_2 is shifted above the BLG valence top and BLG is electron doped. We note that positive electric field points from WSe_2 towards BLG.

Spin splitting of the low energy conduction and valence bands of BLG for the zero and -0.5 V/nm applied electric

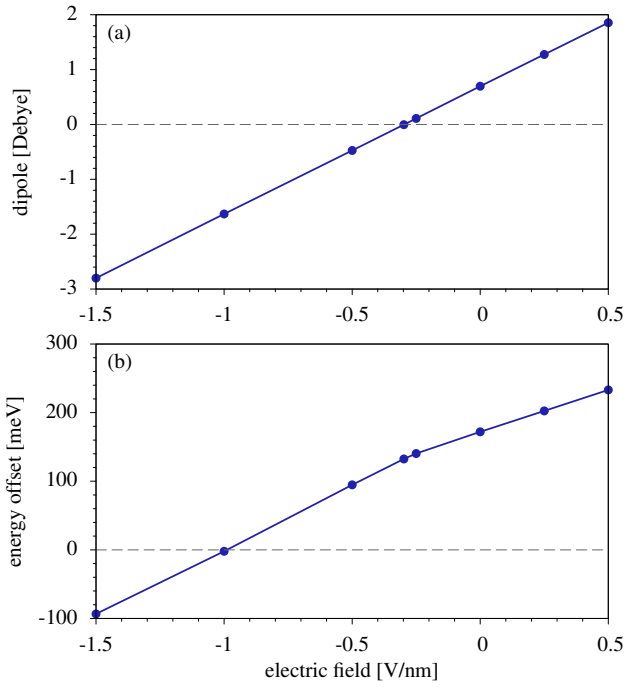


FIG. 7. Calculated electric field dependences in bilayer graphene on WSe_2 of (a) dipole induced in the heterostructure, and (b) energy offset of the bilayer graphene valence band at K point and top of the valence band maximum of the WSe_2 .

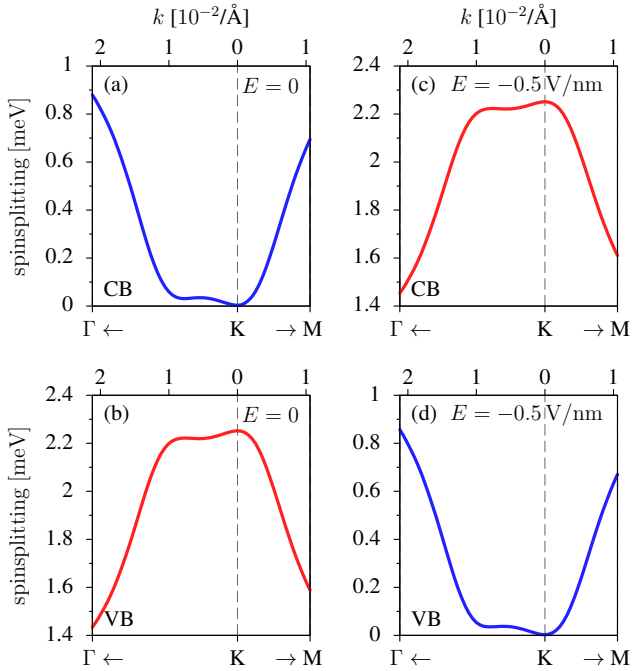


FIG. 8. Calculated spin splitting for low energy bands of bilayer graphene on WSe_2 near the K valley for (a) conduction band (CB) at zero electric field, (b) valence band (VB) at zero field, (c) same as in (a) and (d) same as in (b) but for electric field of -0.5 V/nm.

field are shown in Fig. 8. Comparing the spin splittings within conduction or valence band manifolds, the change in spin splitting around K valley is significant. The minimal values of the spin-orbit splittings are underestimated by Quantum ESPRESSO, as discussed in the paper.